Heliyon 6 (2020) e03759

Contents lists available at ScienceDirect

Heliyon

journal homepage: www.cell.com/heliyon

Research article

Microwave-assisted urea modified crop residue in Cu^{2+} scavenging

A.A. Inyinbor [a,*], F.A. Adekola [b], G.A. Olatunji [b]

[a] Department of Physical Sciences, College of Pure and Applied Sciences, Landmark University, P.M.B 1001, Omu Aran, Nigeria
[b] Department of Chemistry, Faculty of Physical Sciences, University of Ilorin, P.M.B 1515, Ilorin, Nigeria

ARTICLE INFO

Keywords:
Environmental science
Chemistry
Raphia hookeri
Microwave
Surface modification
Adsorption

ABSTRACT

Raphia hookeri fruit epicarp (RHFE) was used in a novel adsorbent preparation via a combination of urea modification and microwave irradiation. The prepared adsorbent (URHFE) was characterized physicochemically, spectroscopically and microscopically characterized. URHFE efficiency in Cu^{2+} scavenging was tested with focus on operational parameters such as pH, dosage, concentration, contact time, ionic strength and temperature. Adsorption data were tested with isotherms and kinetics models. Optimum adsorption occurred at pH of 5.5. The presence of competing ion decreased Cu^{2+} removal and this varied with competing ion concentration. Cu^{2+} uptake decreased with increase in temperature. Percentage desorption was found generally low. The Langmuir monolayer adsorption capacity (q_{max}) was obtained to be 144.93 mg/g, this compared well in effectiveness with other adsorbent previously reported. Dubinin Radushkevich (D-R) isotherm model suggests that adsorption mechanism was chemical in nature. Pseudo second order kinetics best described the adsorption kinetics while multilinear adsorption was observed from the intraparticle diffusion model.

1. Introduction

Pollutants of various category have challenged the environment till now. The inorganic pollutants groups to which heavy metals belong is known to have varying effect on the environment. Heavy metals of all kinds readily enters the aquatic environment via various industrial discharge hence these create the greatest threat to the water environment (Milenkovic et al., 2019). Due to the non-biodegradable nature of heavy metals, they accumulate in the soil, plants and human. Their interactions with human cells results in severe organs damage (Kim et al., 2019).

Heavy metals such as cadmium, mercury, chromium and lead have been grouped as priority control pollutants due to their persistence and irreversible toxicity (USEPA, 2014). Ingestion of high concentration of copper can result in gastrointestinal disruption, gastrointestinal bleeding, hemolytic anemia and respiratory challenges amongst other diseases (Inyinbor et al., 2019; Vardhan et al., 2019). The removal of such priority control pollutant from wastewater is important before their eventual discharge into the environment.

The various conventional methods of heavy metal removal have their accompanying challenges. Adsorption technique, however, is attractive due to its simple operation techniques and efficiency in very low concentration of heavy metal(s) removal (Inyinbor et al., 2016, 2019a; Jafari et al., 2017; Lin et al., 2019; Xiong et al., 2019). The expensive nature of commercial activated carbon is the main challenge associated with adsorption technique. Alternative material to activated carbon in adsorption processes will indeed make adsorption a faultless technique in wastewater treatment (Lin et al., 2019a). Many adsorbents, including polymers composites (Huang et al., 2017), Multiwalled carbon nanotubes (Kheirandish et al., 2017), functioalized nanoparticles (Huang et al., 2017a), coated magnetic nanoparticle (Neeraj et al., 2016), metal organic frameworks (Ghaedi et al., 2018) and Hybrid materials (Huang et al.,2018) have made great adsorbents for pollutants uptake. However, various characteristic features of crop residues make them attractive alternative to activated carbon (Inyinbor et al., 2016, 2017). Crop residues is also of great economic advantage in adsorption when compared with polymers, nanomaterial and metal organic frameworks.

Crop residue of many kinds have been used in metal adsorption (Suganya and Senthil Kumar, 2018; Zhou et al., 2018; Inyinbor et al., 2019; Inyinbor et al., 2019a; Liu et al., 2019). Surface treatment, modification and functionalization can better enhance the adsorption efficiency of crop residues. Modified crop residues such as modified eucalyptus (Kiruba et al., 2014a, 2014b), modified carbon of Pomegranate wood (Ghaedi et al., 2015) and modified caryota urens seeds (Saravanan et al., 2018) have also been used in adsorption of metal ions. In addition to surface modification, microwave irradiation may also create moderate pores on biomass and this treatment is economical

* Corresponding author.
E-mail address: inyinbor.adejumoke@landmarkuniversity.edu.ng (A.A. Inyinbor).

https://doi.org/10.1016/j.heliyon.2020.e03759
Received 8 January 2020; Received in revised form 24 March 2020; Accepted 6 April 2020

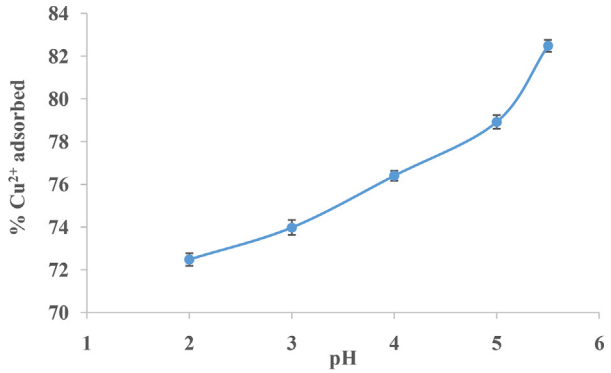

Figure 1. Effects of adsorbate solution pH on Cu^{2+} removal onto URHFE. Conditions: Concentration (60 mg/L), Dosage (1 g/L), Contact time (120 min), Temperature (26 °C) and agitation speed (200 rpm).

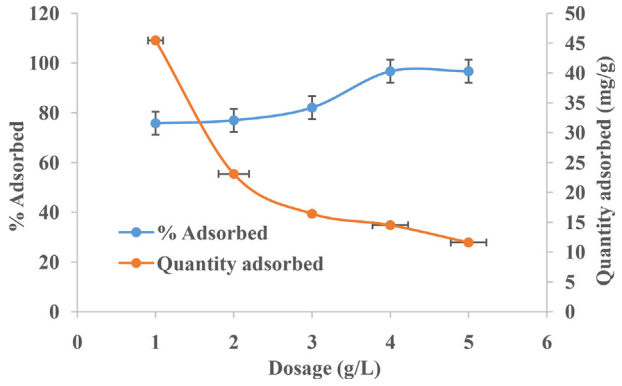

Figure 2. Adsorbent load effects on the uptake of Cu^{2+}onto URHFE. Conditions: Concentration (60 mg/L), pH (5), Contact time (120 min), Temperature (26 °C) and agitation speed (200 rpm).

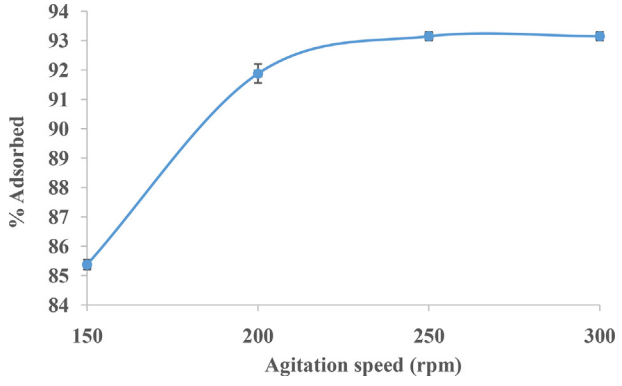

Figure 3. Effects of agitation frequency on Cu^{2+}uptake onto URHFE. Conditions: pH, Concentration, Contact time, Temperature, and dosage are 5, 60 mg/L, 120 min, 26 °C and 1 mg/L respectively.

compared with pyrolysis. Functionalization using amino containing groups such as urea can particularly birth surfaces suitable for metal ion complexation (Wang et al., 2018).

Raphia hookeri is a member of the *palmaceae* family. Wastes from other members of this family viz palm kernel shell and coconut husk have been found effective in pollutant uptake (Baby et al., 2019; Bello et al., 2019). Here, the surface of *Raphia hookeri* fruit epicarp (RHFE) was grafted with nitrogen via urea treatment and porosity subsequently increased via microwave irradiation. This novel adsorbent with enhanced porosity vis-a-vis unique surface was applied in the adsorption

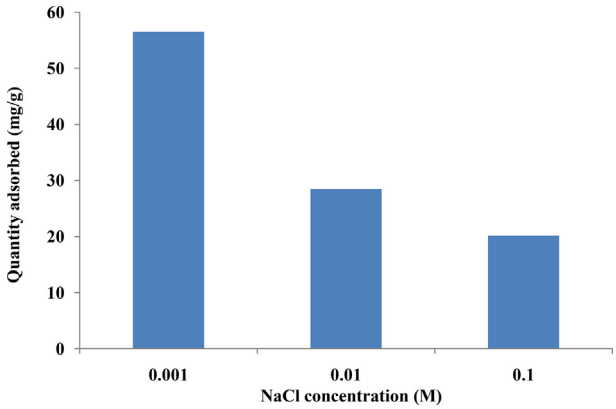

Figure 4. Ionic strength effects of on the Cu^{2+}uptake onto URHFE. Conditions: pH, Concentration, Contact time, Temperature, and dosage are 5, 60 mg/L, 120 min, 26 °C and 1 mg/L respectively.

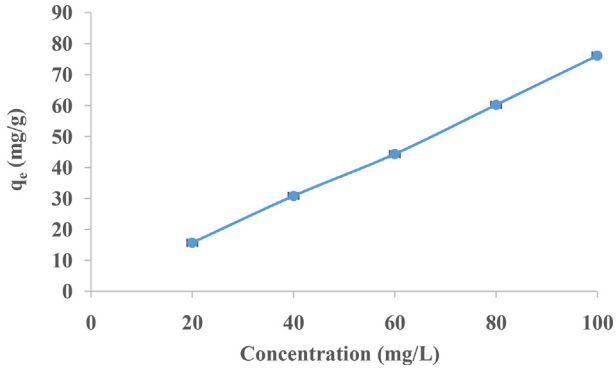

Figure 5. Adsorbate concentration effects on the uptake of Cu^{2+}onto URHFE. Conditions: pH, Contact time, Temperature, and dosage are 5, 120 min, 26 °C and 1 mg/L respectively.

of copper ion in aqueous media. The effects of adsorption operational parameters on Cu^{2+} uptake was well investigated and reported. Until now, no previous report used such uniquely prepared adsorbent in copper removal hence the novelty of this work.

2. Materials and method

2.1. Collection and pretreatment of RHFE

Collection and pretreatment of RHFE is as presented in our recent work (Inyinbor et al., 2019). Briefly, local farmers within Makogi

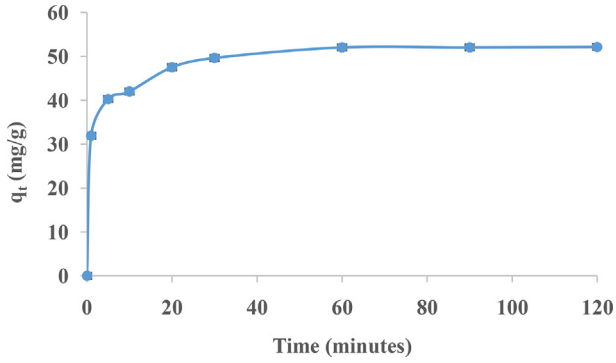

Figure 6. Effects of contact time on the uptake of Cu^{2+}onto URHFE. Conditions: pH, Concentration, Temperature, and dosage are 5, 60 mg/L, 26 °C and 1 mg/L respectively.

Table 1. Isotherm parameters for the uptake of Cu^{2+} onto URHFE.

Isotherms	constants	URHFE
Langmuir	q_{max} (mg/g)	144.93
	K_L (L.mg^{-1})	0.0285
	R_L	0.2597
	R^2	0.9725
Freundlich	K_F	4.16
	n	1.1166
	R^2	0.9907
Temkin	A (L/g)	0.3208
	B	32.889
	b (J/mol)	75.84
	R^2	0.9087
D-R	q_o (mg/g)	59.29
	β(mol^2.kJ^{-2})	0.0052
	E (kJmol^{-1})	9.81
	R^2	0.8512

Table 2. Comparison of URHFE in Cu^{2+} adsorption with others reported in literatures.

Adsorbent	q_o (mg/g)	Reference
Nano supported rubber seed	48.18	Deivasigamani et al. (2017)
Carbon material	3.66	Dai et al. (2017)
Pomegrate peel	30.12	Ben-Ali et al. (2017)
Punai shell activated carbon	57.20	Murugesan et al. (2018)
Municipal waste biochar	4.14	Hoslett et al. (2019)
Gingko leaf	57.80	Lee et al. (2019)
Peanut shell	9.36	Lee et al. (2019)
Metasequoia leave	43.85	Lee et al. (2019)
Modified wheat straw	48.60	Dong et al. (2019)
Acid treated *Cassia fistula* seed biochar	72.90	Hemavathy et al. (2020)
Modified *Raphia* fruit waste	144.93	This study

community, Edu local government of Kwara State supplied *Raphia hookeri* fruits. It was neatly dehulled, the epicarp were collected, washed, dried, pulverized and screen to a specific particle size.

2.2. Microwave irradiation of crop residue

Pretreated RHFE was mixed with urea in a 1:2 m/m ratio. The mixture was exposed to 2450 MHz radiation for 12 min and jelly like paste obtained was subjected to boiling for 30 min, filtered and excess urea washed off with hot water. Further detail is as presented in our previous work (Inyinbor et al., 2017). Functionalized crop residue was labeled URHFE and stored for subsequent studies and usage.

2.3. Adsorbate preparation

Accurately weighed (3.931 g) analar grade of $CuSO_4.5H_2O$ (Lobal Chemie, India) was made into a 1 dm^3 of 1000 ppm Cu^{2+} solution using deionized water. Required lower concentration solutions were then prepared from the stock solution by serial dilution.

2.4. URHFE characteristics

Surface chemistry, morphological appearance as well as physico-chemical parameters of URHFE details have been previously reported (Inyinbor et al., 2017).

2.5. Copper ion adsorption

Various adsorption operational parameters studies including adsorbate initial concentration, adsorbate pH, adsorbent load, agitation speed, system temperature, contact time, as well as other competing ions in solution were carried out. We investigated initial solution pH between 2 and 5.5 considering possible precitation of $Cu(OH)_2$ above this pH. Dosage studies was between 1 to 5 g/L, temperature studies ranged from 40 to 80 °C, agitation speed of 150–300 rpm was investigated while contact time was investigated up to 120 min. To investigate the effects of ionic strength, aqueous solution of NaCl of concentrations 0.1, 0.01 and 0.001 M were used. Generally, 100 cm^3 Cu^{2+} solutions were transferred into plastic bottles containing fixed mass of URHFE, these bottles were properly sealed and subjected to agitation in a thermo regulated shaker operated at specific temperature and speed until equilibrium. Spent adsorbent was filtrated out and the concentrations of unadsorbed metal ion concentration were determined with a Aanalyte 400 atomic absorption spectrophotometer whose detection limit is 0.008 μg/ml. Mathematical relations 1 and 2 were employed for quantity of metal adsorbed at time t and percentage metal ion adsorbed respectively.

$$\boldsymbol{q_t} = \frac{(\boldsymbol{C_i} - \boldsymbol{C_t})}{\boldsymbol{M}} \times \boldsymbol{V} \tag{1}$$

$$\%\ \boldsymbol{Removal} = \frac{(\boldsymbol{C_i} - \boldsymbol{C_t})}{\boldsymbol{C_t}} \times 100 \tag{2}$$

here, C_i is Cu^{2+} initial concentration, C_t is the concentration of Cu^{2+} at time t. V is the volume of Cu^{2+} while M is the mass in g of URHFE.

2.6. Regeneration of spent adsorbent

Effective desorption depicts regeneration and reusability of the spent adsorbent. Ordinary water, 0.1 M CH_3COOH and 0.1 M HCl were used as desorbing reagents. A 0.1 g preloaded adsorbent was dispersed in 100 cm^3 of each eluent which was placed in separate containers. The mixture was tightly closed and subsequently agitated in a thermo specific shaker operated as follows; temperature (26 °C), speed (150 rpm) and time was 120 min. Concentration of Cu^{2+} ion desorbed was determined using AAS, Aanalyte 400. Mathematical Eq. (3) was employed in the calculation of desorption efficiency.

$$\boldsymbol{Desorption\ efficiency}(\%) = \frac{\boldsymbol{q_{de}}}{\boldsymbol{q_{ad}}} \times 100 \tag{3}$$

where q_{de} and q_{ad} are quantity desorbed and quantity adsorbed respectively.

2.7. Adsorption data modeling

2.7.1. Isothermal studies

Isotherm equations viz Langmuir (1916), Freundlich (1906), Temkin (Temkin and Pyzhev, 1940) and Dubinin–Radushkevich (D–R) (Dubinin and Radushkevich, 1947) were employed for equilibrium data modeling. The Langmuir equation and it's dimensionless R_L equations are presented by the mathematical relation 4 and 4a respectively. Expressed Eq. (5) represents linear equation of the Freundlich isotherm, Eq. (6) is the linear equation of Temkin isotherm while the expressed Eq. (7) represents D-R isotherm models linear equation. The Polanyi potential (Ɛ) is presented mathematically in 7a while the mean energy of adsorption (E) is mathematically presented by Eq. (7b).

$$\frac{C_e}{q_e} = \frac{C_e}{q_{max}} + \frac{1}{q_{max} K_L} \tag{4}$$

Table 3. Kinetics data for URHFE-Cu^{2+} adsorption system.

Constants	Adsorbent
	URHFE
$q_{e\ experimental}$ (mg/g)	52.20
Pseudo first order	
$q_{e\ calculated}$ (mg/g)	16.33
K_1 X 10^{-2} (min^{-1})	6.19
R^2	0.9288
SSE	1286.66
X	78.79
Pseudo second order	
$q_{e\ calculated}$ (mg/g)	52.91
K_2 X 10^{-1} ($gmg^{-1}min^{-1}$)	0.11
R^2	0.9998
SSE	0.50
X	0.01
Elovich	
α_{El} (mg/g.min)	6999.50
β_{El} (g/mg)	0.23
R^2	0.9671
Avrami	
n_{Av}	0.44
K_{av} (min^{-1})	0.60
R^2	0.9237
Fractional power	
V (min^{-1})	0.11
K (mg/g)	33.27
KV (mg/g/min)	3.49
R^2	0.9541
Intra particle diffusion	
C_1 (mgg^{-1})	28.74
K_{1diff} ($mgg^{-1}min^{-1/2}$)	4.31
R_1^2	0.9571
C_2 (mgg^{-1})	47.78
K_{2diff} ($mgg^{-1}min^{-1/2}$)	0.44
R_2^2	0.7282

$$R_L = \frac{1}{(1 + K_L C_o)} \quad (4a)$$

$$\text{Log } q_e = \frac{1}{n}\log C_e + \log k_f \quad (5)$$

$$q_e = B\ln A + B\ln C_e \quad (6)$$

$$\ln q_e = \ln q_o - \beta\varepsilon^2 \quad (7)$$

$$\varepsilon = RT\ln\left(1 + \frac{1}{Ce}\right) \quad (7a)$$

$$E = \sqrt{1}\Big/\sqrt{2\beta} \quad (7b)$$

2.7.2. Adsorption kinetics model

Kinetics data were analyzed with pseudo-first-order of Lagergren (Lagergren and Svenska, 1898) whose mathematical relation is expressed in Eq. (8); the pseudo-second-order (Ho and McKay, 1999) which is mathematically expressed by Eq. (9); the Elovich model (Aharoni and Ungarish, 1976), which is expressed mathematically by Eq. (10); the Avrami model (Avrami, 1940), which is mathematically expressed by Eq. (11). The fractional power as well as the Intraparticle diffusion model by Weber and Morris (1963) are mathematically presented with Eqs. (12) and (13) respectively.

$$\ln(q_e - q_t) = \ln q_e - k_1 t \quad (8)$$

$$t/q_t = 1/k_2 q_e^2 + 1(t)/q_e \quad (9)$$

$$q_t = 1/\beta\ln(\alpha\beta) + 1/\beta\ln t \quad (10)$$

$$\ln[-\ln(1-\alpha)] = n_{AV}K_{AV} + n_{AV}lnt \quad (11)$$

$$\log q_t = \log K + v\ log t \quad (12)$$

$$q_t = K_{diff}t^{1/2} + C \quad (13)$$

2.8. Kinetics data validation

Statistical tools viz the Chi square and sum square of error expressed mathematically by Eqs. (14) and (15) respectively were used to validate the kinetics data.

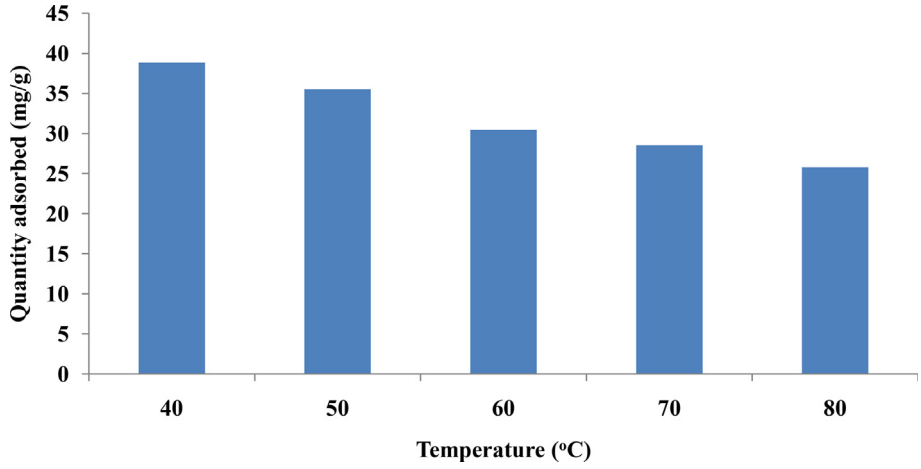

Figure 7. Temperature effects on Cu^{2+}uptake onto URHFE. Conditions: pH, Concentration, Contact time, and dosage are 5, 60 mg/L, 120 min, 26 °C and 1 mg/L respectively.

Table 4. Thermodynamic parameters Cu^{2+}-URHFE system.

Adsorbent	ΔH^o (kJ/mol)	ΔS^o (J/mol/K)	ΔG^o (kJ/mol)				
			313	323	333	343	353
URHFE	-20.76	-61.41	-1.58	-1.00	-0.08	0.28	0.83

$$X^2 = \sum_{i=1}^{n} \frac{(q_{exp} - q_{cal})^2}{q_{cal}} \quad (14)$$

$$SSE = \sum_{i=1}^{n} (q_{cal} - q_{exp})^2 \quad (15)$$

2.9. Thermodynamics of adsorption data

The Gibb's free energy (ΔG^o) giving insight into the spontaneity of adsorption process, the enthalpy of adsorption (ΔH^o) and the adsorption system entropy (ΔS^o) were calculated following mathematical Eqs. (16) and (17).

$$lnK_O = \frac{\Delta S^\circ}{R} - \frac{\Delta H^\circ}{RT} \quad (16)$$

$$\Delta G^\circ = -RTlnK_O \quad (17)$$

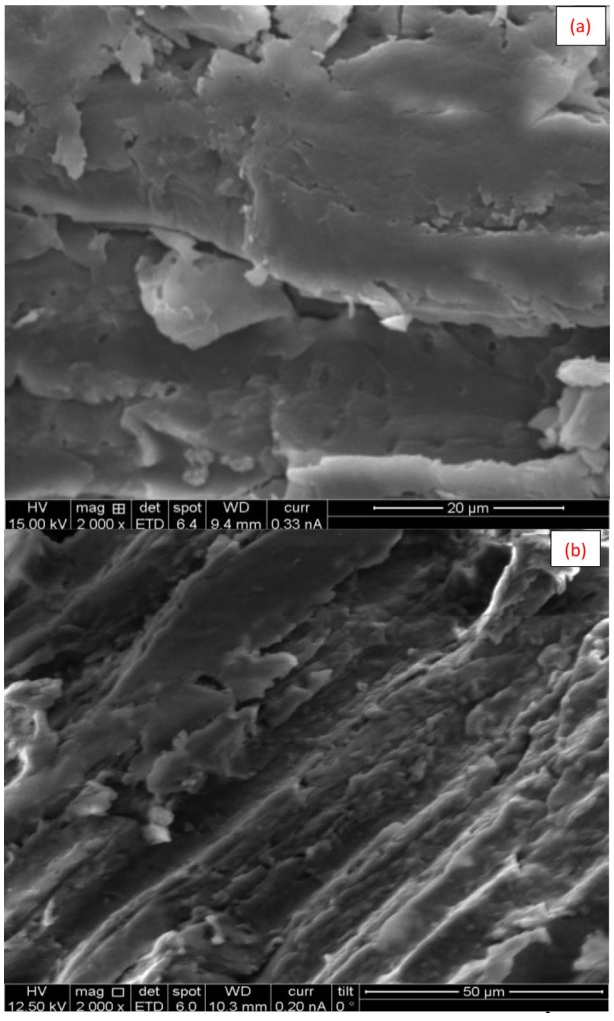

Figure 8. Scanning Electron Microscopic image of URHFE before Cu^{2+} adsorption (a) and after Cu^{2+} adsorption (b).

3. Results and discussion

3.1. URHFE characteristics

Physicochemical parameters of URHFE is as detailed; pH and pHpzc were obtained to be 6.18 and 7.60 respectively. Numerous functional groups often occupy the surface of crop residues hence Brannaur Emmet Teller (BET) surface area was found to be less than 0.001 m^2/g. The available surface functional groups coupled with introduced functional groups will have great use in metal uptake. The adsorbent is carbon rich. In addition to carbon, URHFE also contain 28.68 % oxygen and 0.31 % potassium. Carbon rich materials are excellent adsorbents (Wang et al., 2011).

3.2. Operational parameters' effects on Cu^{2+} adsorption onto URHFE

3.2.1. Effects of pH

Cu^{2+} removal onto URHFE increased gradually with pH. URHFE uptake reached 82.48 % as initial pH of 5.5 (Figure 1). The high concentration of hydroxonium ion at low pH may have resulted in strongly competition of both H_3O^+ and Cu^{2+} for adsorption site at low pH. Hence low uptake of Cu^{2+} at low pH. However, this competition reduces with increased pH since more of H_3O^+ disappears in solution hence more Cu^{2+} found available surface site for adsorption Figure 1.

3.2.2. Dosage effects

Increased adsorbent dose present more sites for adsorbate uptake. However, agglomeration and overlap of adsorbent fixes adsorbent site thus results in non-increase of pollutant uptake. Here, percentage adsorption of Cu^{2+} onto URHFE increased with increase in adsorbent dosage. Adsorption percentage increased up to 4 g/L dosage after which equilibrium was attained (Figure 2). Increase in available adsorption site obviously resulted in increased adsorbent dosage percentage. Adsorbent overlap/aggregation at dosage 4 g/L and above resulted in no further increase in adsorption percentage (Seema et al., 2018; Inyinbor et al., 2019). Quantity adsorbed however was observed to decrease with increase in adsorbent dosage. Quantity adsorbed per unit mass of the adsorbent decreased from 45.44 mg/g to 11.59 mg/g as adsorbent dosage increased from 1 g/L to 5 g/L. Unsaturated adsorption sites in adsorption process may be the justification for decrease in quantity adsorbed (Demirbas et al., 2009). The dosage requirement further justified the economic nature of the prepared adsorbent.

3.2.3. Agitation speed effect on Cu^{2+} uptake onto URHFE

Transfer of Cu^{2+} to the adsorbent active sites may be enhanced by the systems agitation rate. Increased adsorbate-adsorbent collision frequency is expected to enhance Cu^{2+} removal. Percentage Cu^{2+} removal increase with about 5 % more as the agitation speed changed from 150 rpm to 200 rpm (Figure 3). Further increase of about 2 % was observed as the speed increased to 250 rpm. Agitation speed beyond 250 rpm did not in any way further increased percentage adsorption. The rate of bombardment of Cu^{2+} to the surface of URHFE may facilitate higher Cu^{2+} removal.

3.2.4. Ionic strength effects on Cu^{2+} uptake onto URHFE

Various ion may be present in wastewater depending on their source hence the importance of ionic strength effect. In specifics is the presence of salts in various wastewater. Here, Na^+ of varying concentrations was introduced in order to increase the Cu^{2+} solution ionic strength in this study. Presence of Na^+ affected the uptake of Cu^{2+} onto URHFE with

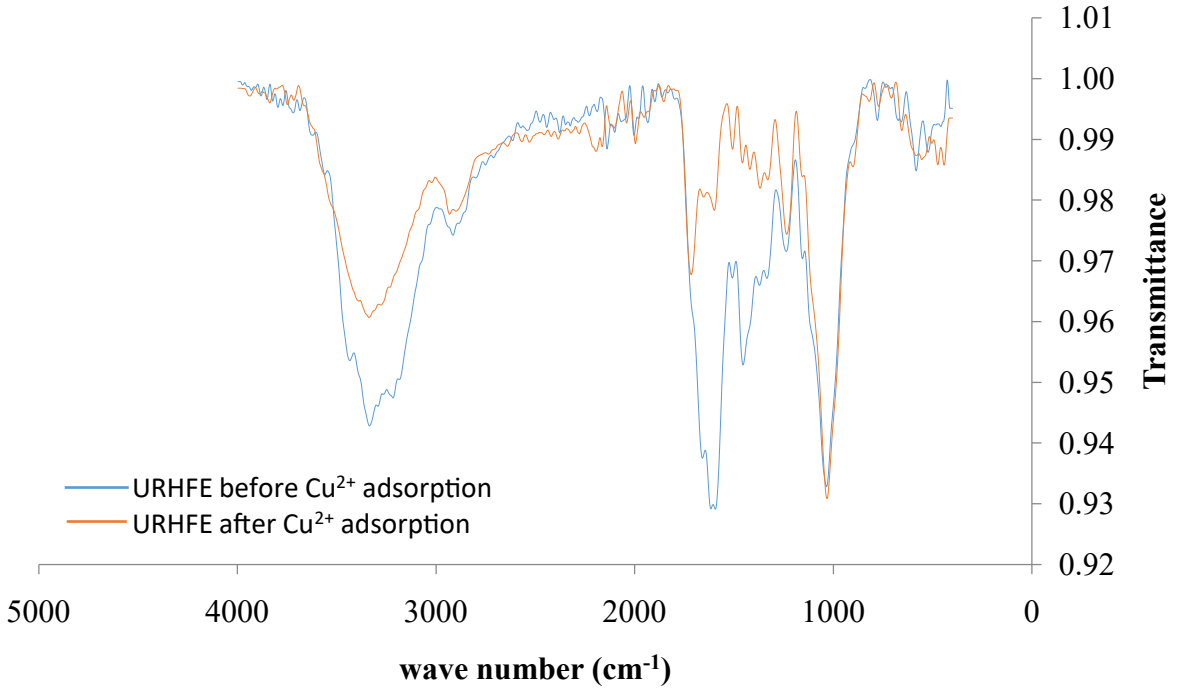

Figure 9. FTIR spectral of URHFE before and after Cu^{2+} uptake.

respect to Na^{+} concentration (Figure 4). The effect was observed to be negligible at the lowest concentration studied while quantity removed decreased with increase in Na^{+} ion. Decrease in quantity Cu^{2+} adsorbed with increase in Na^{+} concentration suggest a strong repulsive force between the adsorbent surface adsorptive ions as well as site competition between Cu^{2+} and Na^{+} (Keshtkar et al., 2019).

3.2.5. Initial Cu^{2+} load effects

High concentration is known to supply high driving resulting in aqueous-solid barrier breakdown consequently more Cu^{2+} is transferred to the adsorbent surface at high concentration. Here, removal percentage ranged between 73 and 78 % across concentrations studied (Figure 5) with higher percentage removal at higher concentration.

3.2.6. Effect of contact time on Cu^{2+} uptake onto URHFE

URHFE site was observed to be highly active thus Cu^{2+} adsorption was rapid with about 70 % of the total Cu^{2+} in solution removed within the first 10 min. Slight increase was subsequently observed in quantity removed then equilibrium was attained at 60 min and above (Figure 6).

Quantity of Cu^{2+} adsorbed at equilibrium was obtained to be 52.2 mg/g. Many available adsorption site at time zero may have been responsible for rapid initial Cu^{2+} uptake. Usually, huge vacant adsorption sites results in wide concentration gradient between the adsorbate in solution and adsorbent sites hence rapid initial adsorption. Subsequent pore penetration of adsorbate into the pores of the adsorbent results into the slow adsorbate uptake (Mnasri-Ghnimi and Frini-Srasra, 2019). Adsorption sites are gradually covered as time progressed hence adsorption rate decreased significantly as mass transfer of adsorbate from the aqueous solution reduces.

3.3. Isothermal studies of Cu^{2+} adsorption onto URHFE

Correlation coefficient obtained for the Freundlich isotherm (0.9907) suggests that uptake of Cu^{2+} onto URHFE was onto multiple sites. Favourable adsorption was indicated as the Freundlich constant n was greater than 1 (Table 1). The q_{max} for Cu^{2+} uptake onto URHFE was 144.93 mg/g suggesting a better efficiency than many adsorbent reported in literature. Some level of adsorbate-adsorbate interaction may also have occurred in the Cu^{2+}-URHFE system as Temkin R^2 value was obtained to be 0.9087. The Temkin constant b was obtained to be greater than 40 kJ/mol and energy of adsorption E obtained from the D-R model was found to be greater 8 kJ/mol. These observations suggest that the uptake of Cu^{2+} onto URHFE may be by chemical method which suggests that Cu^{2+} may be by complexation (Kenawy et al., 2019). URHFE performance in the current adsorption was compared with others previous reports and URHFE was found to very efficient (Table 2). The energy of adsorption was obtained to be greater than 8 kJ/mol suggesting that chemisorption dominates URHFE-Cu^{2+} adsorption system.

3.4. Kinetics studies of Cu^{2+} adsorption onto URHFE

The importance of kinetics studies is in establishment of adsorption mechanism (Pourebrahim et al., 2017). In the case of pseudo second order kinetics, calculated quantity adsorbed compared closely with experimental obtained quantity adsorbed (Table 3). The correlation coefficient also tends to unity while SSE and X^2 values were very low. All aforementioned indicates that the pseudo second order best described Cu^{2+} uptake unto URHFE. This further reiterate that chemisorption dominate the URHFE-Cu^{2+} system (Ofomaja et al., 2010). In the case of the pseudo first order kinetics however, statistical calculation gave very high values and calculated quantity greatly deviates from experimentally obtained quantity at equilibrium. For the intraparticle diffusion model plot, a multiple linear profile was obtained (Figure not shown), these indicates that adsorption occurred in two stages (Inyinbor et al., 2016a). The initial steep part shows the fast diffusion of copper ions towards URHFE surface while the gradual adsorbate pore penetration is depicted by the second part. The diffusion rate was observed to increase from the first part while the boundary thickness increased, however, intraparticle diffusion was not the rate controlling step as the graph of q_t versus $t^{1/2}$ did not pass through the origin (Figure not shown).

3.5. Temperature effects and thermodynamics studies

URHFE was more stable and very efficient at lower system temperature. Its removal efficiency decreased with increasing temperature from 30 °C to 80 °C (Figure 7). Possibility of agro waste fiber breakdown may

exist hence reducing surface adsorption site and consequently adsorption efficiency. ΔG^o values across temperature also corroborate URHFE efficiency variation with temperature (Table 4). Positive ΔG^o values were obtained at higher temperature. The fact that ΔH^o was obtained to be less than zero suggests that excess energy in bond formation than bond breaking were released in the form of heat (Zhang et al., 2020). Negative values of ΔG^o at low temperature suggests that adsorption process was spontaneous and feasible at low temperature, however at high temperature adsorbent performance reduced greatly. This may be as a results of biomass breakdown. Degree of disorderliness at the solid-liquid interphase was in a decreasing order since ΔS^o was less than zero.

3.6. Insight into URHFE reusability

Percentage desorption was obtained to be very low for all the eluents used, negligible percentage of 0.08 % was obtained for HCl, while neutral water and CH_3COOH gave percentage desorption of 6.27 and 6.30 % respectively. Low percentage desorption depicts Cu^{2+} stability on URHFE surface. CH_3COOH gave the highest desorption percentage, suggesting that chemical adsorption of Cu^{2+} was predominant. This could be as a result of complex formation via interactions of donor atoms site and vacant metal d-orbital.

3.7. Post adsorption characterization of URHFE

URHFE was characterized with a smooth surface, non uniform pores and gullies (Figure 8 a). Its fibrous nature can also be seen vividly. All of these characteristics are suitable for pollutants uptake. URHFE after Cu^{2+} adsorption showed swollen fibers with Cu^{2+} overlay were seen (Figure 8 b). The shift and reduction in intensity of carbonyl and amino stretching vibrations indicates that these functional groups participated in Cu^{2+} uptake (Figure 9).

4. Conclusion

Selectively treated crop residue applied for the adsorption of Cu^{2+} was found highly effective having removal efficiency up to 82.48 % at optimum pH. High temperature broke down fibers and adsorption sites of URHFE hence low temperature gave better adsorption efficiency. The intraparticle modeling of the adsorption data gave a multilinear profile indicating that adsorption of Cu^{2+} onto URHFE was in stages. Freundlich isotherm ascertain a multilayer adsorption with correlation coefficient close to unity. The q_{max} was 144.93 mg/g and URHFE was found more efficient than other crop residue reported in literature.

Declarations

Author contribution statement

Adejumoke Inyinbor, Folahan Adekola: Conceived and designed the experiments; Performed the experiments; Analyzed and interpreted the data; Contributed reagents, materials, analysis tools or data; Wrote the paper.

Gabriel Olatunji: Conceived and designed the experiments; Performed the experiments; Analyzed and interpreted the data; Contributed reagents, materials, analysis tools or data.

Funding statement

This research did not receive any specific grant from funding agencies in the public, commercial, or not-for-profit sectors.

Competing interest statement

The authors declare no conflict of interest.

Additional information

No additional information is available for this paper.

References

Aharoni, C., Ungarish, M., 1976. Kinetics of activated chemisorptions. Part I: the non- Elovichian part of the isotherm. J. Chem. Soc. Faraday Trans. 72, 265–268.

Avrami, M., 1940. Kinetics of phase change: transformation-time relations for random distribution of nuclei. J. Chem. Phys. 8, 212–224.

Baby, R., Saifullah, B., Hussein, M.Z., 2019. Palm Kernel Shell as an effective adsorbent for the treatment of heavy metal contaminated water. Sci. Rep. 9, 18955.

Bello, O.S., Adegoke, K.A., Fagbenro, S.O., Lameed, O.S., 2019. Functionalized coconut husks for rhodamine-B dye sequestration. Appl. Water Sci. 9, 189.

Ben-Ali, S., Jaouali, I., Souissi-Najar, S., Ouederni, A., 2017. Characterization and adsorption capacity of raw pomegranate peel biosorbent for copper removal. J. Clean. Prod. 142, 3809–3821.

Dai, Y., Zhang, K., Li, J., Jiang, Y., Chen, Y., Tanaka, S., 2017. Adsorption of copper and zinconto carbon material in an aqueous solution oxidized by ammonium peroxydisulphate. Separ. Purif. Technol. 186, 255–263.

Deivasigamani, P., Rangasamy, P., Senthil Kumar, P., Saravanan, A., Reni, J., Tani, T., 2017. Sorption of Cu (II) ions by nano-scale zerovalent iron supported on rubber seed shell. IET Nanobiotechnol. 11 (6), 714–724.

Demirbas, E., Dizge, N., Sulak, M.T., Koby, M., 2009. Adsorption kinetics and equilibrium of copper from aqueous solutions using hazelnut shell activated carbon. Chem. Eng. J. 148, 480–48.

Dong, J., Du, Y., Duyu, R., Shang, Y., Zhang, S., Han, R., 2019. Adsorption of copper ion from solution by polyethylenimine modified wheat straw. Bioresour. Technol. Rep. 6, 96–102.

Dubinin, M.M., Radushkevich, L.V., 1947. Equation of the characteristic curve of activated Charcoal. Proc. Acad. Sci. Phys. Chem. USSR 55, 331–333.

Freundlich, H.M.F., 1906. Over the adsorption in solution. Zeitschrift für Physikalische Chemie 57, 385–470.

Ghaedi, A.M., Ghaedi, M., Vafaei, A., Iravani, N., Keshavarz, M., Rada, M., Tyagi, I., Agarwal, S., Gupta, V.K., 2015. Adsorption of copper (II) using modified activated carbon prepared from Pomegranate wood: optimization by bee algorithm and response surface methodology. J. Mol. Liq. 206, 195–206.

Ghaedi, A.M., Panahimehr, M., Nejad, A.R.S., Hosseini, S.J., Vafaei, A., Baneshi, M.M., 2018. Factorial experimental design for the optimization of highly selective adsorption removal of lead and copper ions using metal organic framework MOF-2 (Cd). J. Mol. Liq. 272, 15–26.

Hemavathy, R.V., Senthil Kumar, P., Kanmani, K., Jahnavi, N., 2020. Adsorptive separation of Cu (II) ions from aqueous medium using thermally/chemically treated Cassia fistula based biochar. J. Clean. Prod. 249, 119390.

Ho, Y.S., McKay, G., 1999. Pseudo-second order model for sorption processes. Process Biochem. 34, 451–465.

Hoslett, J., Ghazal, H., Ahmad, D., Jouhara, H., 2019. Removal of copper ions from aqueous solution using low temperature biochar derived from the pyrolysis of municipal solid waste. Sci. Total Environ. 673, 777–789.

Huang, Q., Liu, M., Chen, J., Wan, Q., Tian, J., Huang, L., Jiang, R., Wen, Y., Zhanga, X., Wei, Y., 2017. Facile preparation of MoS_2 based polymer composites via mussel inspired chemistry and their high efficiency for removal of organic dyes. Appl. Surf. Sci. 419, 35–44.

Huang, Q., Liu, Q., Mao, L., Xu, D., Zeng, G., Huang, H., Jiang, R., Deng, F., Zhang, X., Wei, Y., 2017a. Surface functionalized SiO2 nanoparticles with cationic polymers via the combination of mussel inspired chemistry and surface initiated atom transfer radical polymerization: characterization and enhanced removal of organic dye. J. Colloid Interface Sci. 499, 170–179.

Huang, Q., Liu, M., Zhaa, J., Chena, J., Zeng, G., Huang, H., Tian, J., Wen, Y., Zhang, X., Wei, Y., 2018. Facile preparation of polyethylenimine-tannins coated SiO_2 hybridmaterials for Cu^{2+} removal. Appl. Surf. Sci. 427, 535–544.

Inyinbor, A.A., Adekola, F.A., Olatunji, G.A., 2016. Kinetic and thermodynamic modeling of liquid phase adsorption of Rhodamine B dye onto *Raphia hookerie* fruit epicarp. Water Resour. Ind. 15, 14–27.

Inyinbor, A.A., Adekola, F.A., Olatunji, G.A., 2016a. Liquid phase adsorption of Rhodamine B onto acid treated *Raphia hookerie* epicarp: kinetics, Isotherm and thermodynamics studies. S. Afr. J. Chem. 69, 218–226.

Inyinbor, A.A., Adekola, F.A., Olatunji, G.A., 2017. Kinetics and Isothermal modeling of liquid phase adsorption of Rhodamine B onto Urea modified *Raphia hookerie* epicarp. Appl. Water Sci. 7, 3257–3266.

Inyinbor, A.A., Adekola, F.A., Olatunji, G.A., 2019. Copper scavenging effiency of adsorbents prepared from *Raphia hookeri* fruit waste. Sustain. Pharm. 12, 100141.

Inyinbor, A.A., Adekola, F.A., Dada, A.O., Oluyori, A.P., Olatunji, G.A., Fanawopo, O.F., Oreofe, T.A., Abodunrin, T.O., 2019a. Novel acid treated biomass: applications in Cu2+ scavenging, Rhodamine B/Cu2+ binary solution and real textile effluent treatment. Environ. Technol. Innov. 13, 37–47.

Jafari, M., Rahimi, M.R., Ghaedi, M., Kheibar Dashtian, K., 2017. ZnO nanoparticles loaded different mesh size of porous activated carbon prepared from Pinus eldarica and its effects on simultaneous removal of dyes: multivariate optimization. Chem. Eng. Res. Des. 125, 408–421.

Kenawy, I.M.M., Eldefrawy, M.M., Eltabey, R.M., Zaki, E.G., 2019. Melamine grafted chitosan-montmorillonite nanocomposite for ferricions adsorption: central composite design optimization study. J. Clean. Prod. 241, 118189.

Keshtkar, A.R., Moosavian, M.A., Sohbatzadeh, H., Mofras, M., 2019. La(III) and Ce(III) biosorption on sulfur functionalized marine brown algae Cystoseira indica by xanthation method: response surface methodology, isotherm and kinetic study. Groundwater Sustain. Dev. 8, 144–155.

Kheirandish, S., Ghaedi, M., Dashtian, K., Heidari, F., Pourebrahim, F., Wang, S., 2017. Chitosan extraction from lobster shells and its grafted withfunctionalized MWCNT for simultaneous removal of Pb^{2+} ions anderiochrome cyanine R dye after their complexation. Int. J. Biol. Macromol. 102, 181–191.

Kim, J., Kim, Y., Kumar, V., 2019. Heavy metal toxicity: an update of chelating therapeutic strategies. J. Trace Elem. Med. Biol. 54, 226–231.

Kiruba, U.P., Kumar, P., Prabhakaran, C., Adity, V., 2014a. Characteristics of thermodynamic, isotherm, kinetic, mechanism and design equations for the analysis of adsorption in Cd (II) ions-surface modified Eucalyptus seeds system. J. Taiwan Inst. Chem. Eng. 45, 2957–2968.

Kiruba, U.P., Senthil Kumar, P., Gayatri, K.S., Hameed, S.S., Sindhuja, M., Prabhakaran, C., 2014b. Study of adsorption kinetic, mechanism, isotherm, thermodynamic, and design models for Cu(II) ions on sulfuric acid-modified Eucalyptus seeds: temperature effect. Desalination Water Treat. 56 (11), 2948–2965.

Langmuir, I., 1916. The constitutional and fundamental properties of solids and liquids. J. Am. Chem. Soc. 38, 2221–2295.

Lagergren, S., Svenska, B.K., 1898. On the theory of so-called adsorption of materials. R. Swedish Acad. Sci. Doc B*and* 24, 1–13.

Lee, M., Park, J.H., Chung, J.W., 2019. Comparison of the lead and copper adsorption capacities of plant source materials and their biochars. J. Environ. Manag. 236, 118–124.

Lin, G., Wang, S., Zhang, L., Hu, T., Cheng, S., Fu, L., Xiong, C., 2019. Enhanced and selective adsorption of Hg^{2+} to a trace level using trithiocyanuric acid-functionalized corn bract. Environ. Pollut. 244, 938–946.

Lin, G., Hu, T., Wang, S., Xie, T., Zhang, L., Cheng, S., Fu, L., Xiong, C., 2019a. Selective removal behavior and mechanism of trace Hg(II) using modified corn husk leaves. Chemosphere 225, 65–72.

Liu, J., Hu, C., Huang, Q., 2019. Adsorption of Cu^{2+}, Pb^{2+}, and Cd^{2+} onto oil tea shell from water. Bioresour. Technol. 271, 487–491.

Milenkovic, B., Stajic, J.M., Stojic, N., Pucarevic, M., Strbac, S., 2019. Evaluation of heavy metals and radionuclides in fish and sea food products. Chemosphere 229, 324–331.

Mnasri-Ghnimi, S., Frini-Srasra, N., 2019. Removal of heavy metals from aqueous solutions by adsorption using single and mixed pillared clays. Appl. Clay Sci. 179, 105151.

Murugesan, A., Divakaran, M., Senthilkumar, P., 2018. Enhanced adsorption of Cu^{2+}, Ni^{2+}, Cd^{2+} and Zn^{2+} ions onto physico-chemically modified agricultural waste: kinetic, isotherm and thermodynamic studies. Desalination Water Treat 122, 176–191.

Neeraj, G., Krishnan, S., Senthil Kumar, P., Shriaishvarya, K.R., Vinoth Kumar, V., 2016. Performance study on sequestration of copper ions from contaminated water using newly synthesized high effective chitosan coated magnetic nanoparticles. J. Mol. Liq. 214, 335–346.

Ofomaja, A.E., Naidoo, E.B., Modise, S.J., 2010. Dynamic studies and pseudo-second order modeling of copper(II) biosorption ontopine cone powder. Desalination 251, 112–122.

Pourebrahim, F., Ghaedi, M., Dashtian, K., Heidari, F., Kheirandish, S., 2017. Simultaneous removing of Pb^{2+} ions and alizarin red S dye after their complexation by ultrasonic waves coupled adsorption process: spectrophotometry detection and optimization study. Ultrason. Sonochem. 35, 51–60.

Saravanan, A., Senthil Kumar, P., Renita, A.A., 2018. Hybrid synthesis of novel material through acid modification followed ultrasonication to improve adsorption capacity for zinc removal. J. Clean. Prod. 172, 92–105.

Seema, K.M., Mamba, B.B., Njuguna, J., Bakhtizin, R.Z., Mishra, A.K., 2018. Removal of lead (II) from aqueous waste using (CD-PCL-TiO2) bio-nanocomposites. Int. J. Biol. Macromol. 109, 136–142.

Suganya, S., Senthil Kumar, P., 2018. Influence of ultrasonic waves on preparation of active carbon from coffee waste for the reclamation of effluents containing Cr(VI) ions. J. Ind. Eng. Chem. 60, 418–430.

Temkin, M.I., Pyzhev, V., 1940. Kinetics of ammonia synthesis on promoted iron catalyst. Acta Physiochim. USSR 12, 327–356.

USEPA, 2014. Priority pollutant list. available on. https://www.epa.gov/sites/production/files/2015-09/documents/priority-pollutant-list-.

Vardhan, K.H., Kumar, P.S., Panda, R.C., 2019. A review on heavy metal pollution, toxicity and remedial measures: current trends and future perspectives. J. Mol. Liq. 290, 111197.

Wang, X.J., Wang, Y., Wang, X., Liu, M., Xia, S.Q., Yin, D.Q., Zhang, Y.L., Zhao, J.F., 2011. Microwave-assisted preparation of bamboo charcoal-based iron containing adsorbents for Cr(VI) removal. Chem. Eng. J. 174, 326–332.

Wang, L., Yan, W., He, C., Wen, H., Cai, Z., Wang, Z., Chen, Z., Liu, W., 2018. Microwave-assisted preparation of nitrogen-doped biochars by ammonium acetate activation for adsorption of acid red 18. Appl. Surf. Sci. 433, 222–231.

Weber, W.J., Morris, J.C., 1963. Kinetics of adsorption on carbon from solution. J. Sanity Eng. Div. Am. Soc. Civil Eng. 89, 31–59.

Xiong, C., Wang, S., Sun, W., Li, Y., 2019. Selective adsorption of Pb (II) from aqueous solution using nanosilica functionalized with diethanolamine: equilibrium, kinetic and thermodynamic. Microchem. J. 146, 270–278.

Zhang, X., Xue, Y., Gao, J., He, C., Ji, Y., Dou, Y., 2020. Comparison of adsorption mechanisms for cadmium removal by modified zeolites and sands coated with Zn-layered double hydroxides. Chem. Eng. J. 380, 122578.

Zhou, Z., Xu, Z., Feng, Q., Yao, D., Yu, J., Wang, D., Lv, S., Liu, Y., Zhou, N., Zhong, M., 2018. Effect of pyrolysis condition on the adsorption mechanism of lead, cadmium and copper on tobacco stem biochar. J. Clean. Prod. 187, 996–1005.